J. Biochem. 2010;147(6):905–915 doi:10.1093/jb/mvq029

JB THE JOURNAL OF BIOCHEMISTRY

Structure of metallo-β-lactamase IND-7 from a *Chryseobacterium indologenes* clinical isolate at 1.65-Å resolution

Received January 24, 2010; accepted February 26, 2010; published online March 19, 2010

Yoshihiro Yamaguchi[1,*,†], Nobutoshi Takashio[2], Jun-ichi Wachino[3], Yuriko Yamagata[4], Yoshichika Arakawa[3], Koki Matsuda[2] and Hiromasa Kurosaki[2,*,†]

[1]Environmental Safety Center, Kumamoto University, 39-1 Kurokami 2-Chome, Kumamoto 860-8555, Japan; [2]Department of Structure-Function Physical Chemistry, Graduate School of Pharmaceutical Sciences, Kumamoto University, Oe-honmachi 5-1, Kumamoto 862-0973, Japan; [3]Department of Bacterial Pathogenesis and Infection Control, National Institute of Infectious Diseases, 4-7-1 Gakuen, Musashi-Murayama, Tokyo 208-0011, Japan; and [4]Department of Structural Biology, Graduate School of Pharmaceutical Sciences, Kumamoto University, Oe-honmachi 5-1, Kumamoto 862-0973, Japan

*Yoshihiro Yamaguchi, Environmental Safety Center, Kumamoto University, 39-1 Kurokami 2-Chome, Kumamoto 860-8555, Japan. Tel: +81 96 342 3238, Fax: +81 96 342 3237, email: yyamagu@gpo.kumamoto-u.ac.jp

*Hiromasa Kurosaki, Department of Structure-Function Physical Chemistry, Graduate School of Pharmaceutical Sciences, Kumamoto University, O-e honmachi 5-1, Kumamoto 862 0973, Japan. Tel/Fax: +81 96 371 4314, email: ayasaya@gpo.kumamoto-u.ac.jp

†These authors contributed equally to the work.

The X-ray crystal structure of metallo-β-lactamase from *Chryseobacterium indologenes* IND-7 was determined at a resolution of 1.65 Å. The overall structure adopted a four-layered αβ/βα sandwich structure with a dinuclear zinc(II) active site, in which the zinc(II) ions were denoted as Zn1 and Zn2. The overall structure of IND-7 is analogous to those of subclass B1 metallo-β-lactamases, as determined by X-ray crystallography. A significant structural difference, however, was observed in the dinuclear zinc(II) active site: the coordination geometry around Zn1 changed from tetrahedral, found in other subclass B1 metallo-β-lactamases, to distorted trigonal bipyramidal, whereas that of Zn2 changed from trigonal bipyramidal to tetrahedral. Arg121(101), which is located in the vicinity of the dinuclear zinc(II) active site, may affect the binding affinity of Zn2 due to an electronic repulsion between the zinc(II) ion(s) and a positively charged guanidyl group of Arg121(101). Moreover, the hydrogen-bonding interaction of Arg121 with Ser71(53), which is conserved in IND-1, IND-3 and IND-5–IND-7, appeared to have important consequences for the binding affinity of Zn2 in conjunction with the above electrostatic effect.

Keywords: β-lactams/metallo-β-lactamase/crystal structure/X-ray crystallography/zinc(II).

Abbreviations: BBL, class B β-lactamase; BcII, metallo-β-lactamase from *Bacillus cereus*; BlaB, metallo-β-lactamase from *Cryseobacterium meningosepticum*; CcrA, metallo-β-lactamase from *Bacteroides fragilis*; GIM-1, metallo-β-lactamase from *Pseudomonas aeruginosa*; IMP-1, metallo-β-lactamase from *Serratia marcescens*; IND-1, IND-2, IND-2a, IND-3, IND-4, IND-5, IND-6 and IND-7; metallo-β-lactamases from *Chryseobacterium indologenes*; PDB, Protein Data Bank; SIM-1, metallo-β-lactamase from *Acinetobacter baumannii*; SPM-1, metallo-β-lactamase from *Pseudomonas aeruginosa*; VIM-2, metallo-β-lactamase from *Pseudomonas aeruginosa*.

Metallo-β-lactamases are zinc(II)-dependent enzymes that catalyze the hydrolysis of the amide bond in most β-lactams, including carbapenems, and are associated with one of the prevalent mechanisms of bacterial resistance against β-lactams (*1–3*). Metallo-β-lactamases (referred to as class B β-lactamases) are grouped into the molecular subclasses B1 – B3 based on their primary amino acid sequence (*4–6*). Subclasses B1 and B2 metallo-β-lactamases have the amino acid sequences, H*X*H*X*D and N*X*H*X*D, respectively. Subclass B3 metallo-β-lactamases have the amino acid sequence H(Q)*X*H*X*DH. Subclasses B1 and B3 metallo-β-lactamases are able to bind up to two zinc(II) ions (*7–10*) and can hydrolyze a wide range of β-lactams including penicillins, cefalosporins and carbapenems (*11*). On the other hand, subclass B2 metallo-β-lactamases are mononuclear zinc(II) enzymes, which exhibit specificity toward carbapenems (*11–17*).

Among them, subclass B1 metallo-β-lactamases are gaining popularity worldwide, and their genes are encoded either on the bacterial chromosome or on mobile genetic elements such as plasmids and transposons (*6*, *18–20*). For instance, chromosomally encoded metallo-β-lactamases include BcII from *Bacillus cereus* (*21*), BlaB from *Chryseobacterium meningosepticum* (*22*), CcrA from *Bacteroides fragilis* (*23*) and IND-1 from *Chryseobacterium indologenes* (*24*), whereas IMP-1 from *Serratia marcescens* (*25*), VIM-2 from *Pseudomonas aeruginosa* (*18*), SPM-1 from *P. aeruginosa* (*26*), SIM-1 from *Acinetobacter*

baumannii, and GIM-1 from *P. aeruginosa* (*27*) are encoded by mobile genes on a plasmid. So far, the three-dimensional structures of the subclass B1 metallo-β-lactamases have been solved for BcII (*7*, *28*–*30*), BlaB (*31*), CcrA (*32*–*34*), IMP-1 (*35*, *36*), VIM-2 (*37*, *38*) and SPM-1 (*10*).

In 1999, the chromosome-encoded *C. indologenes* metallo-β-lactamase IND-1 was first isolated (*24*), and six IND variants, designated IND-2 to IND-6 and IND-2a, have been detected to date (*39*–*41*). *Chryseobacterium indologenes* are aetiological agents of infection associated with the use of indwelling devices (*42*). The amino acid sequences of the above-mentioned six IND variants share 72–92% identity with that of IND-1 (Fig. 1). Of these enzymes, kinetic parameters are available for IND-1, IND-2, IND-5 and IND-6, though in the case of IND-1, only a comparison of the K_m values is available (*24*, *39*–*41*).

In 2005, Arakawa *et al.* isolated a chromosomal metallo-β-lactamase produced by a *C. indologenes* clinical isolate from the urinary tract infection of a patient in Japan (MRY040066 strain). Based on a comparison of the amino acid sequence of metallo-β-lactamase from *C. indologenes* MRY040066 (denoted as IND-7) with that of IND-1, IND-7 identified most with IND-1 (99%) where an isoleucine at position 90(72) in IND-1 was replaced by a valine in IND-7. (In this paper, the amino acid residues are designated by a BBL numbering (*4*), and the amino acid sequence number from the N-terminus for mature protein—the latter is in parenthesis.)

The aim of this study is to fully characterize the three-dimensional structure of IND-7 from *C. indologenes*, because the X-ray crystal structures of IND variants are not available. We report here the crystal structure of metallo-β-lactamase IND-7 at a resolution of 1.65 Å.

Materials and Methods

Cloning

The bla_{IND-7} gene was amplified with the primers IND-F (5′-CAT ATG AAA AAA AGC ATC CGT TTT-3′), which have an NdeI linker (underlined), and IND-R (5′-GGA TCC CTA TTT TTT ATT CAG AAG TT-3′), which have a BamHI linker (underlined), using an Expand High-Fidelity PCR system (Roche). The template DNA was extracted from the clinically isolated *C. indologenes* strain MRY040066. The amplicon was ligated with a pGEM-T vector (Promega), and was partially excised by digestion with NdeI and BamHI. The excised fragment was subcloned into the expression vector pET29a(+) (Novagen) to yield plasmid pET29a(+)/bla_{IND-7}.

Expression and purification

A 25-ml overnight preculture of *Escherichia coli* BL21(DE3), which was transformed by plasmid pET29a(+)/bla_{IND-7}, was used to inoculate 10 l of LB broth supplemented with 50 μg/ml kanamycin, and the resulting culture was grown at 37°C with shaking until the culture reached an OD_{600} of about 1.0. The culture was developed in 0.1 mM isopropyl-β-D-thiogalactopyranoside (IPTG) and shaken at 37°C for 2 h. The culture was centrifuged at 5,000 *g* for 10 min at 4°C. The pellets (about 40 g, wet weight) were washed by resuspension in 40 ml of 20 mM Tris–HCl pH 7.4, with repeat centrifugation. The pellets were resuspended in 40 ml of the same buffer, disrupted by sonication for 5 min and centrifuged at 100,000 *g* for 75 min at 4°C. After removal of insoluble components by filtration (MILLEX-GP 0.45 μm, Millipore), the filtrate was loaded into an SP Sepharose Fast Flow column (ϕ 2.6 × 10 cm, GE Healthcare) pre-equilibrated with 20 mM Tris–HCl pH 7.4, and the proteins were eluted with a linear gradient of 0–0.5 M NaCl. Fractions were analysed by sodium dodecyl sulphate polyacrylamide gel electrophoresis (SDS-PAGE) and by their ability to turn over nitrocefin as a substrate. Fractions containing the desired activity were pooled and concentrated to a volume of 10 ml by Ultracel YM-10 (Millipore). The concentrated protein was loaded into a Sepharose G-75 column (ϕ 1.6 × 10 cm, GE Healthcare) and was eluted with 20 mM Tris–HCl pH 7.4 containing 0.3 M NaCl. Fractions containing the IND-7 protein were pooled and concentrated to a volume of 6 ml. The protein was then reloaded into a Sephacryl HR-100 column (ϕ 1.6 × 10 cm, GE Healthcare) and was eluted with 20 mM Tris–HCl pH 7.4 containing 0.3 M NaCl. The protein was further concentrated to 14 mg/ml using both Ultracel YM-10 (Millipore) and Amicon Ultra-15 (Millipore). The purity of the IND-7 protein was estimated to be greater than 95% by SDS-PAGE at a protein concentration of 1 mg/ml. Prior to the X-ray diffraction experiments, a buffer solution of the IND-7 protein was converted from 20 mM Tris–HCl containing 0.3 M NaCl to 20 mM HEPES–NaOH pH 7.5. For crystallization, the purified IND-7 protein was concentrated to about 14 mg/ml using both Amicon YM-10 (Millipore) and Amicon Ultra (Millipore).

Crystallization

Screening for IND-7 crystallization conditions was performed at 20°C by the hanging-drop method using Crystal Screen and Crystal Screen II kits (Hampton Research): drops mixed 2 μl of a protein solution with 2 μl of a reservoir solution. The best crystals suitable for X-ray diffraction study were obtained from condition No. 17 using the Crystal Screen kit [30%(w/v) PEG4000, 0.1 M Tris–HCl pH 8.5 and 0.2 M Lithium sulphate monohydrate], which grew as plates within 3 months at 20°C.

Data collection and refinement

All diffraction data were collected at 100 K after cryoprotection by a brief exposure to a reservoir solution containing 30% (w/v) PEG4000 at the SPring-8 (Harima, Japan) and the Photon Factory (Tsukuba, Japan). The data set used the structural analysis that was collected at the SPring-8 on a beamline 38B1 (Harima, Japan) at a resolution of 1.65 Å and a wavelength of λ = 1.00 Å. Data for the crystal were integrated, merged, and scaled using HKL-2000 (*43*). The refined structure (PDB code: 1M2X) of BlaB from *C. meningosepticum* at a 1.5 Å resolution (*31*) was used as the search model for molecular replacement using the AMoRe (*44*) and Molrep (*45*) software programs, which are a component of the CCP4 program suite v.6.0.0 (*46*). The interactive graphics programs O (*47*) and Coot v.0.1.2 (*48*) were used to build the IND-7 structure (*47*). The refinement was performed with the CNS (*49*) and Refmac (*50*) software programs. Data collection and refinement statistics are listed in Table I. Selected bond distances and angles are shown in Table II.

PDB Accession Code

The atomic coordinates and structure factors have been deposited in the Protein Data Bank under accession code 3L6N.

Nucleotide Sequence Accession Number

The nucleotide sequence encoding IND-7 characterized in this study appears in the EMBL/GenBank/DDBJ databases under accession AB529520.

Results and Discussion

Overall structure of IND-7

The structure of IND-7 from *C. indologenes* was solved by molecular replacement. The final refined structural model contained residues Gln38(21)–Lys293(238), two zinc(II) ions (Zn1 and Zn2), two sulphate ions, and 327 ordered water molecules per asymmetric unit, and was refined to $R_{working} = 17.7\%$ and $R_{free} = 20.0\%$ at 1.65 Å resolution (Table I). The root mean square differences (RMSD) from the ideal

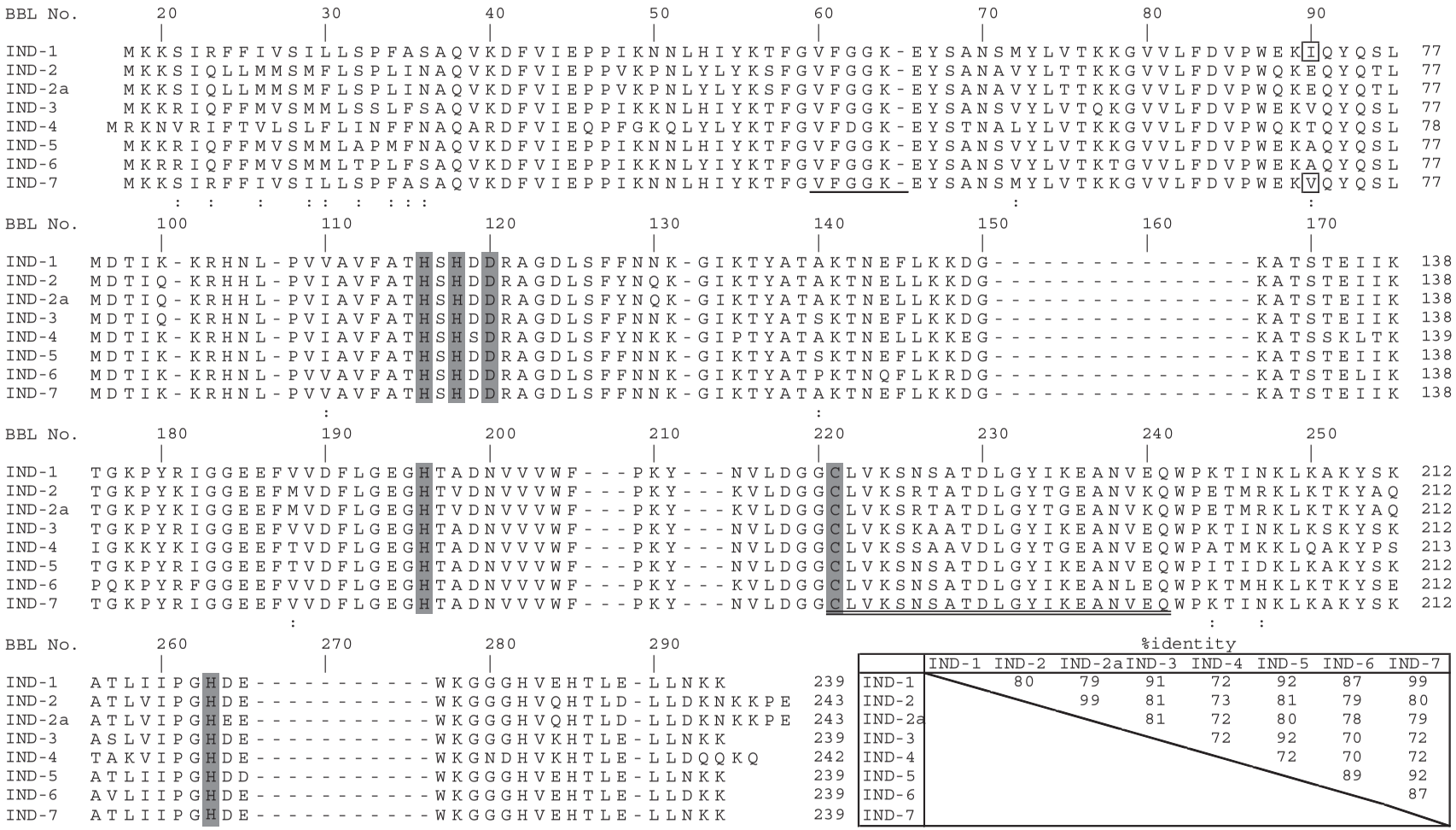

Fig. 1 Alignment of the amino acid sequence of IND-7 from *C. indologenes* with those of seven IND variants from *C. indologenes*. The IND variants are as follows: IND-1 (GenBank accession number: AF099139), IND-2 (AF219129), IND-2a (AF219130), IND-3 (AF219133), IND-4 (AF219135), IND-5 (AY504627) and IND-6 (AM087455). Sequence comparison was performed by aligning the protein amino acid sequences by use of the MULTALIN program (*66*). The class B metallo-β-lactamase numbering scheme is indicated above the sequences (*4*). Dashes indicate gaps introduced to optimize the alignment. Numbers on the right indicate numbers of amino acid residues from the N-terminus for each mature protein. Zinc(II)-coordinating residues are shaded in grey. Substitutions between IND-1 and IND-7 are circled. Substitutions between IND-5 and IND-7 are indicated by colons. The regions of loop 1 and loop 2 in IND-7 are underlined and double-underlined, respectively. The matrix at the bottom of the figure summarizes the levels of amino acid sequence identity.

Table I. Data collection and refinement statistics for IND-7.

Data collection	
Resolution (Å)	50.0−1.65 (1.71−1.65)
Wavelength (Å)	1.00
Unit-cell parameters (Å, °)	$a=77.6$, $b=74.3$, $c=47.4$, $\beta=99.4$
Space group	$C2$
Redundancy	3.7 (3.5)
Completeness (%)	99.9 (99.7)
R_{merge}[a]	4.3 (0.104)
No. of unique reflections	31,928 (901)
$I/\sigma(I)>$	48.5 (16.7)
Refinement statistics	
σcut-off	None
Resolution (Å)	38.3−1.65 (1.69−1.65)
No. of reflections used	30,314
B factors (Å^2)	
Average	13.5
Protein	11.0
Water	26.0
No. of non-H atoms[b]	
Protein	1,811
Water	327
R.m.s. deviation for ideal[c]	
Bond lengths (Å)	0.008
Angles (°)	1.09
$R_{working}$[d]	0.177 (0.221)
R_{free}[e]	0.200 (0.250)

[a] $R_{merge}=\sum_{hkl}\sum_i|I_i(hkl)-<I(hkl)>|/\sum_{hkl}\sum_i I_i(hkl)$, where $I_i(hkl)$ is the observed intensity for reflection for hkl and $<I(hkl)>$ is the average intensity calculated for reflection hkl from replicate data. [b]Per asymmetric unit. [c]RMSD.: root mean square differences. [d] $R_{working}=\sum_{hkl}||F_o|-|F_c||/\sum_{hkl}|F_o|$, where F_o and F_c are the observed and calculated structure factors, respectively. [e] $R_{free}=\sum_{hkl}||F_o|-|F_c||/\sum_{hkl}|F_o|$ for 5% of the data not used at any stage of structural refinement. Values in parentheses are for the last resolution shell.

bond distances and angles were 0.008 Å and 1.09°, respectively. A Ramachandran plot showed that 97.6% and 5.8% of the residues were in the most-favoured regions and in the additionally allowed regions, respectively, and 0.5% and 1.1% of those were in the generously allowed regions and in the disallowed regions, respectively. The exceptions were Asp50(33) and Asp84(66), which adopted ϕ and ψ angles of 79° and −51°, and 70° and 160°, respectively. Asp84 was buried in the protein and exhibited a strained main chain conformation, which is a commonly observed feature in the crystal structures of BcII, CcrA and IMP-1 metallo-β-lactamases (*28*, *32*, *35*). Therefore, it is thought that conservation of the conformation of Asp84 is important to the folding of metallo-β-lactamases.

The overall structure of IND-7 was found to be composed of five α-helixes and twelve β-strands, which fold into a four-layered αβ/βα sandwich structure (Fig. 2A). The dinuclear zinc(II) active site was located at the bottom of a shallow groove and was made up of the two zinc(II) ions (Zn1 and Zn2), the zinc(II) ion binding residues and two loops (loop 1 and loop 2). Loop 1, which is a typical feature of subclass B1 metallo-β-lactamases, was formed by residues at positions 60−66 (*51*) (BBL numbering, Figs 1 and 2A) between β2 and β3. This flexible loop is thought to be responsible for the tight binding of substrates and inhibitors in the dinuclear zinc(II) active site (*35*, *51*–*55*). In the IND-7 structure, loop 1 was well defined. Loop 2 was comprised residues at positions 221−241 (BBL numbering), positioned approximately opposite loop 1 cantered at about the zinc(II) binding site (Figs 1 and 2A). Thus, the overall structure of IND-7 was found to be similar to the previously solved structures of subclass B1 metallo-β-lactamases (*7*, *10*, *28*–*38*).

Coordination mode and occupancy of zinc(II) ions in the dinuclear zinc(II) active site

To understand the structural features of IND-7 in detail, the structures of IND-7 and structurally well-characterized CcrA from *B. fragilis*, which have 28% sequence homology (PDB code: 1ZNB; 1.85 Å resolution), were compared. As shown in Fig. 2B, superimposing the Cα atoms of IND-7 and molecule A in CcrA demonstrated a similarity in the protein folds with an overall RMSD of 1.7 Å, as mentioned above. Despite the similarity in the overall structures between these two enzymes, noticeable structural differences were found in the dinuclear zinc(II) active sites.

In the CcrA structure (Fig. 3A), Zn1 was coordinated with His116(99), His118(101), His196(162) and a water molecule or hydroxide ion (Wat1), forming a tetrahedral geometry, whereas Zn2 was coordinated with Asp120(103), Cys221(181), His263(223), one water molecule (Wat3, termed 'apical water') and Wat1, forming a trigonal bipyramidal geometry. The zinc(II) coordination geometry found in CcrA is mostly conserved in subclass B1 metallo-β-lactamases.

On the other hand, the zinc(II) coordination mode of IND-7 was different from the common feature. In the process of refinement of the IND-7 structure, we initially set the occupancies of Zn1 and Zn2 as 1.0 and refined their B-factors. As the B-factor of Zn2 (15.6 Å^2) was relatively higher than that of Zn1 (9.3 Å^2), occupancies for Zn1 and Zn2 were reset as 1.0 and 0.7, respectively, for subsequent refinement. The final B-factors equalled ~9.3 Å^2 for Zn1 and 12.3 Å^2 for Zn2. The average B-factor of the residues involved in the zinc(II) coordination, His116(96), His118(98), Asp120(100), His196(159), Cys221(178) and His263(220), was 7.1 Å^2. These results suggested that the affinity of Zn2 was lower than that of Zn1, and that Zn2 tended to escape from the dinuclear zinc(II) active site of IND-7 Moreover, a $2|F_o|-|F_c|$ electron density map around the Zn2 site (Fig. 3B) clearly showed the existence of both conformations in the side chains of Cys221(178) and His263(220), where the occupancies of Cys221A(178) and His263A(220) were refined by 0.7, and those of Cys221B(178) and His263B(220) were refined by 0.3. The former was a Zn2-coordinated form, whereas the latter was a Zn2-uncoordinated form. Interestingly, in the side chain of Asp120(100), a zinc(II) ligand, no disorder was observed, which was fixed through the interactions of Zn2 and Wat1 (*vide infra*). This finding indicates that Asp120 played an important role in helping to orient a zinc(II)-bound hydroxide ion for a nucleophilic attack on the CO group of the β-lactam ring.

The coordination geometry around Zn1 (Fig. 3B) was a distorted trigonal bipyramid with $\tau=0.88$

Table II. Zinc(II)-ligand distances (Å) and angles (°) for IND-7 and CcrA metallo-β-lactamases.

		IND-7	CcrA[a]	
Zn(II)-ligand[b]		Distances		
Zn1	His116NE2	2.1	2.1/2.2	
	His118ND1	2.0	2.0/2.1	
	His196NE2	2.0	2.0/2.0	
	O(Wat1)	1.9	1.9/2.0	
	O(Wat2)	2.6		
Zn2	Asp120OD2	2.1	2.3/2.1	
	Cys221ASG	2.2	2.3/2.4	
	His263ANE2	2.1	2.1/2.2	
	O(Wat1)	2.1	2.1/2.2	
	O(Wat3)		2.3/2.2	
Zn1	Zn2	3.6	3.5/3.5	
Ligand-Zn(II)-Ligand[b]			Angles	
His116(96)NE2	Zn1	His118ND1	99	105/100
	Zn1	His196NE2	102	100/106
	Zn1	O(Wat1)	108	119/111
His118(98)ND1	Zn1	His196NE2	116	107/108
	Zn1	O(Wat1)	116	112/109
His196(159)NE2	Zn1	O(Wat1)	113	113/121
O(Wat2)	Zn1	His116NE2	169	
	Zn1	His118ND1	71	
	Zn1	His196NE2	88	
	Zn1	O(Wat1)	73	
Asp120(100)OD2	Zn2	Cys221ASG	113	97/97
	Zn2	His263ANE2	91	86/82
	Zn2	O(Wat1)	94	86/81
Cys221A(179)SG	Zn2	His263ANE2	110	107/110
	Zn2	O(Wat1)	118	115/117
His263A(220)NE2	Zn2	O(Wat1)	125	138/132
O(Wat3)	Zn2	Asp120OD2		161/164
	Zn2	Cys221ASG		101/110
	Zn2	His263ANE2		83/89
	Zn2	O(Wat1)		92/95

[a]The distances and angles for CcrA metallo-β-lactamase are quoted for molecules A and B in the asymmetric unit. [b]Ligand numbers are indicated by the BBL numbering scheme and numbers of amino acid resides from the N-terminus for each mature protein are omitted for simplification.

[structural parameter $\tau = (\beta - \alpha)/60$) (*56*)], where $\alpha = 116^\circ$ for His118(98)ND1−Zn1 − His196(159)NE2 and $\beta = 169^\circ$ for O(Wat2) − Zn1 − His116(96)NE2 were the two basal angles ($\beta \geq \alpha$) representing the change in trigonal distortion from a square pyramidal geometry: $\tau = 0$ for an ideal square pyramid and 1 for an ideal trigonal bipyramid. Two His residues, His118(98) and His196(159), and either one oxygen from a water molecule or a hydroxide ion (labeled Wat1) made a trigonal plane (the average angle of the corresponding angles was 115°). Wat1, which is thought to act as the attacking nucleophile on the CO group of the β-lactam ring (*32*, *57*, *58*), bridged to both Zn1 and Zn2, and also formed a hydrogen bond with one oxygen atom of Asp120(100) with a distance of 2.7 Å. The apical positions were occupied by His116(96) and Wat2, where Wat2 weakly interacted with Zn1 at a distance of 2.6 Å [the average Zn − Wat bond distance in zinc(II) enzymes is reportedly 2.2 Å (*59*)]. In the crystal structure of VIM-2 metallo-β-lactamase, Zn1 is also coordinated to five ligands in a distorted trigonal bipyramidal geometry (*37*), as seen in the IND-7 structure. However, the Zn1 − Wat bond distance (2.8 Å) at the apical position was longer by 0.2 Å than that of IND-7 (Zn1 − Wat2). These observations suggest that Wat2 can more easily accommodate replacement by the Zn1 coordination sphere upon uptake of substrates and inhibitors. We expected the coordination structure of the dinuclear zinc(II) active site in IND-7, especially pentacoordination at the Zn1 site, to be of major benefit to a favourable Michaelis complex, because Wat2 was thought to be the carbonyl oxygen atom of the β-lactam ring that interacted with Zn1 upon formation of the Michaelis complex (Fig. 4).

The Zn1−His and Zn1−Wat1 bond distances were 2.0 − 2.1 Å and 1.9 Å, respectively, which were almost identical to those found in CcrA (2.0 − 2.2 Å for Zn1 − His and 1.9 − 2.0 Å for Zn1 − O, respectively). Zn2 was tetrahedrally coordinated with Asp120(100), Cys221A(178), His263A(220), and Wat1, with bond distances of 2.1 Å (Fig. 3B), and 'the apical water Wat3', observed in CcrA, was missing from the IND-7 structure. The Zn2 − Wat1 bond distance of 2.1 Å was somewhat longer than that of Zn1−Wat1 and this tendency was also found in CcrA. The ligand−Zn2−ligand bond angles of 91−125° (the average angle; 109°) were close to the optimal tetrahedral angles. The Zn1 − Zn2 distance was 3.6 Å and this bond distance was close to that of CcrA (3.5 Å). Thus, the zinc(II) coordination geometry was notably

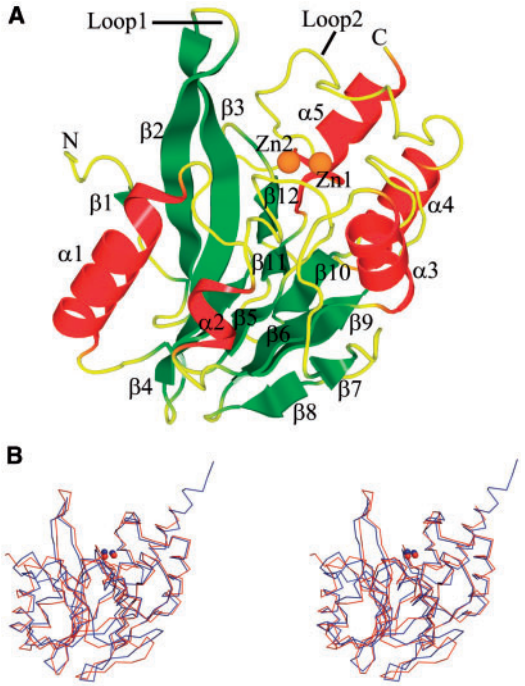

Fig. 2 Overall structure of IND-7 from *C. indologenes*. (A) A ribbon diagram of IND-7 is shown with the secondary structures labeled. α-Helices, β-strands and the loops are shown in red, green and yellow, respectively. Zinc(II) ions are represented as orange spheres. The figure was prepared with MolFeat software (FiatLux Corporation). (B) Superposition of the C_α tracing of IND-7 (red) with CcrA from *B. fragilis* [blue, PDB code: 1ZNB, (*32*)]. In the CcrA structure, only molecule A is depicted.

different from those of other crystal structures of subclass B1 metallo-β-lactamases, which includes CcrA.

Role of Arg121 and hydrogen-bonding networks around the dinuclear zinc(II) active site

Arg121 is well conserved in IND variants (*39*, *40*), VIM variants (*20*), BlaB (*60*) and BcII (*7*, *32*), and is thought to be responsible for the reduced binding affinity for Zn2 (*29*, *33*, *35*). Indeed, BcII metallo-β-lactamase has a binding affinity that differs from that of the two zinc(II) binding sites (*61–63*). By contrast, residues at position 121 in CcrA and IMP variants are occupied by Cys121(104) and Ser121(82), respectively, and these metallo-β-lactamases display high binding affinity at both the Zn1 and Zn2 sites (*64*, *65*).

As seen in Fig. 3C, a positively charged guanidinyl group of Arg121(101) was situated below the floor of the Zn2 site. A $2|F_o| - |F_c|$ electron density map clearly indicated Arg121(101) alternated in the crystal, and the conformations Arg121A(101) and Arg121B(101) fit the map well. The former corresponded to a Zn2-coordinated form of Cys221(178) and His263(220), whereas the latter corresponded to a Zn2-uncoordinated form with no bound Zn2. Therefore, the corresponding atoms in the two conformations were refined with occupancies of 0.7 and 0.3, respectively. In Arg121A(101), the electrostatic repulsion between a positively charged bulky guanidinyl group of Arg121 and Zn2 cause movement of the guanidinyl group to move away from Zn2 [4.7 Å from Arg121A(101)NE and 5.7 Å from Arg121A(101)NH2], where the guanidinyl group is maintained by four hydrogen bonds between Asn70(52), Ser71(*53*), Asp84(66) and Asp120(100): Arg121A(101)NE Asp120(100)O = 2.8 Å, Arg121A(101)NH1 · Asp84(66)OD2 = 3.2 Å, Arg121A(101)NH2 · Asn70(52) = 2.7 Å and Arg121A(101)NH2 · Ser71(*53*)OG = 3.0 Å. Ser71(53) is conserved in IND-1, IND-3, and IND-5–IND-7 but is Gly in IND-2, IND-2a, and IND-4 (Fig. 1). The substitution of residues at position 71(*53*) in IND variants is expected to have an effect on the changing of the binding affinity of Zn2 and on the hydrolysis of β-lactams.

In Arg121B(101), with a rotation of the CG–CD bond of the side chain in Arg121B(101), the plane formed by the atoms CD, NE, NH1 and NH2 of Arg121B(101) was nearly perpendicular to the corresponding plane of Arg121A(101) and the guanidinyl group of Arg121B(101) lay close to the dinuclear zinc(II) active site [3.5 Å from Arg121B(101)NE and 3.6 Å from Arg121B(101)NH2]. The guanidinyl group made four hydrogen bonds with Asn70(*52*), Asp84(66), Asp120(100) and Gly262(219): Arg121B(101)NE Asp120(100)OD2 = 2.9 Å, Arg121B(101)NH1 Asn70(52)O = 3.0 Å, Arg121B(101)NH1 Asp84(66)OD2 = 3.2 Å and Arg121B(101)NH2 Gly262(219)O = 2.7 Å, of which two hydrogen bonds of Arg121B(101) with Asp120(100) and Gly262(219) pulled the guanidinyl group close to the dinuclear zinc(II) active site. These observations highlight the importance of Arg121(101) for the binding affinity of Zn2 by cooperation between the electrostatic effect and the change in the hydrogen-bonding network. In addition, Arg121(101) also appeared to partially contribute to the preservation of the moderate orientation of Asp120(100) relative to Zn2.

We compared the hydrogen-bonding networks around the dinuclear zinc(II) active site to estimate the primary cause of the differences in coordination structure between IND-7 and CcrA metallo-β-lactamases.

In CcrA, the side chain NZ of Lys224(184) produced hydrogen-bonding networks with Wat3 coordinated to Zn2, the side chain ND1 of His196(162), and the main chain oxygen atoms of Cys221(181), Ile231(191) and Asn233(193) through well-ordered water molecules (Fig. 5A). Lys224 located on loop 2 was assumed to interact with the carboxylate of the β-lactams (*32*, *35*). Moreover, the side chain of ND2 of Asn233(193) formed a hydrogen-bonding network with bridging water between Zn1 and Zn2, Wat1, via a water molecule. Conversely, the hydrogen-bonding networks in IND-7 were somewhat different from those of CcrA (Fig. 5B). Lys224(181), which was ~7 Å away from the zinc(II) active site, did not participate in the hydrogen-bonding networks between the bulk water molecules. In the case of IND-7, Asn233(193) in CcrA was replaced with Tyr233(190), which was located on loop 2. Tyr233(190) rotated ~74° around the CB–CG bond and the hydroxy group of the phenyl ring was ~8 Å away from Zn1. The main chain oxygen atoms of Leu231(188) and Tyr233(190) were hydrogen bonded to a water molecule, which is

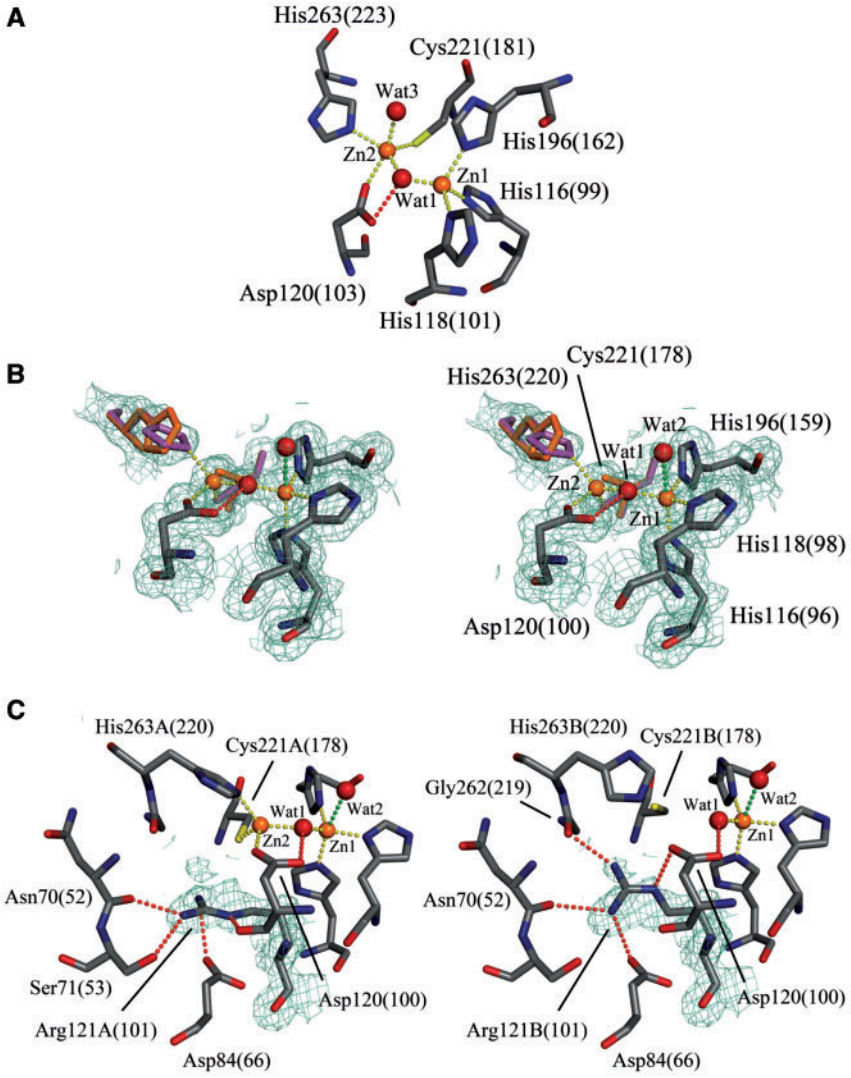

Fig. 3 Comparison of the dinuclear zinc(II) active site structures in CcrA from *B. fragilis* [PDB code: 1ZNB, (32)] and IND-7 from *C. indologenes*. (A) Active site structure in CcrA; only molecule A is depicted. Zn1 is tetrahedrally coordinated with His116(99), His118(101), His196(162) and Wat1. Zn2 is trigonal-bipyramidally coordinated with Asp120(103), Cys221(181), His263(223), Wat1 and Wat2. Zinc(II) ions and water molecules are presented as orange and red spheres, respectively. Carbon, oxygen, nitrogen and sulphur atoms are shown in grey, red, blue and yellow, respectively. Zn(II) – ligand bonds are shown as yellow dotted lines. The hydrogen bond is shown as a red dotted line. (B) Stereo view of the active site in IND-7. The electron density map (green mesh) is shown contoured at the 1.0σ level in the $2|F_o|-|F_c|$ map. Zinc(II) ions and water molecules are shown as orange and red spheres, respectively. Carbon, oxygen, nitrogen and sulphur atoms are shown in grey, red, blue and yellow, respectively. Zn(II)–ligand bonds, with the exception of the Zn(II)–Wat2 bond, are shown as yellow dotted lines. The Zn(II)–Wat2 bond is shown as a green dotted line. The hydrogen bond is shown as a red dotted line. The occupancies of Zn1 and Zn2 are refined with 1.0 and 0.7, respectively. Cys221(178) and His263(220) adopted alternative conformations in the IND-7 structure [Cys221A(178) and His263A(220), and Cys221B(178) and His263B(220)]. The occupancies of Cys221A(178) and His263A(220) (magenta sticks) are refined with 0.7 in each case, whereas those of Cys221B(178) and His263B(220) (orange sticks) are refined with 0.3 in each. Zn1 is trigonal-bipyramidally coordinated with His116(96), His118(98), His196(159), Wat1 and Wat2. Zn2 is tetrahedrally coordinated with Asp120(100), Cys221A(178), His263A(220) and Wat1. Unlike the CcrA structure, 'the apical water' Wat3 is absent from the Zn2 site. (C) Alternative conformations of Arg121(101), Arg121A(101) and Arg121B(101). The electron density map (green mesh) of Arg121(101) is shown contoured at the 1.0σ level in $2|F_o|-|F_c|$ map. Of the two conformations, Arg121A(101) is shown to the left, whereas Arg121B(101) is shown to the right. The former was a Zn2-coordinated form of Cys221(178) and His263(220), whereas the latter was a Zn2-uncoordinated form with no bound Zn2. The occupancies of Arg121A(101) and Arg121B(101) are refined with 0.7 and 0.3, respectively. Carbon, oxygen, nitrogen and sulphur atoms are shown in grey, red, blue and yellow, respectively. Zn(II)–ligand bonds, with the exception of Zn(II)–Wat2, are shown as yellow dotted lines. The Zn(II)–Wat2 bond is shown as a green dotted line. Hydrogen bonds are shown as red dotted lines. The figures were prepared with *PyMol* software (http://pymol.sourceforgen.net/).

occupied in a position equivalent to that of a water molecule in the CcrA structure, forming hydrogen-bonding networks with Wat1 and Wat2 that was coordinated to Zn1, the side chain ND1 of His196(159), and the main chain oxygen atoms of Cys221(181). Interestingly, Wat2 formed two hydrogen bonds with two water molecules, one of which interacted with Wat1 to achieve formation of a hydrogen-bonding network between Wat1 and Wat2—the other was linked to bulk water molecules. This seemed to be one of the factors affecting the structural change in the Zn1 coordination sphere, which was also thought to be closely related to the difference in enzymatic activity.

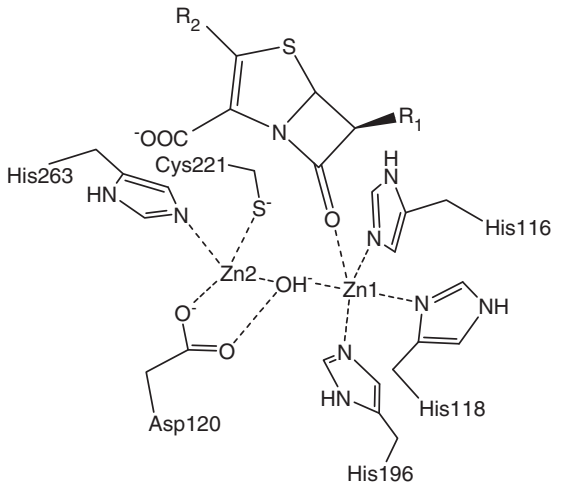

Fig. 4 A model of the Michaelis complex for β-lactam bound to subclass B1 metallo-β-lactamase.

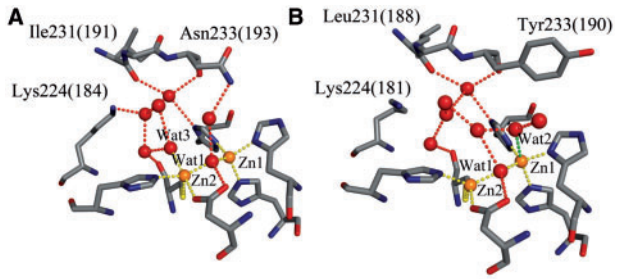

Fig. 5 Comparison of hydrogen-bonding networks between (A) CcrA from *B. fragilis* [PDB code: 1ZNB, (32)] and (B) IND-7 *C. indologenes* in the vicinity of the dinuclear zinc(II) active sites. Carbon, oxygen, nitrogen and sulphur atoms are shown in grey, red, blue and yellow, respectively. Zn(II)–ligand bonds, with the exception of Zn(II)–Wat2, are shown as yellow dotted lines. The Zn(II)–Wat2 bond is shown as a green dotted line. Hydrogen bonds are shown as red dotted lines. The figures were prepared with *PyMol* software (http://pymol.sourceforgen.net/).

Structure-activity relationship between IND-2 and IND-5 deduced from the IND-7 structure

In 2007, Perilli *et al*. (*40*) isolated IND-5 from a clinical isolate of *C. indologenes* and conducted kinetic studies on the hydrolysis of various β-lactams against IND-5 metallo-β-lactamase. From a comparison of kinetic parameters of IND-5 with those of IND-2, they reported that the catalytic efficiencies (k_{cat}/K_m) of IND-2 for imipenem and meropenem were ~25- and 13-fold higher than those of IND-5, respectively. On the basis of the comparison of the amino acid sequence of IND-5 with those of IND variants, including IND-2, Perilli *et al*. assumed that the residue at position 265 (BBL numbering) might be involved in the drastic reduction in catalytic efficiency of IND-5, compared with that of IND-2 (*39*, *40*): Glu265(222) was well conserved in all IND variants with the exception of IND-5 [in this case, Asp265(222)] and was located close to His263(220), which is a Zn2 ligand.

As shown in Fig. 1, IND-7 shared 92% amino acid identity with the IND-5 of sixteen amino acid substitutions: Ser21(4)Lys, Lys23(6)Tyr, Ile26(9)Met, Ile29(12)Met, Leu30(13)Met, Ser32(15)Ala, Phe34(17)Met, Ala35(*18*)Phe and Ser36(19)Asn in the signal peptide region; and, Met72(54)Val, Val90(72)Ala, Val110(90)Ile, Ala140(119)Ser, Val188(151)Thr, Lys244(201)Ile, Asn247(204)Asp and Glu265(222)Asp. Extrapolating from the determined IND-7 structure, most of the amino acid substitutions of IND-5 were expected to be located either on the surface of the protein or far from the active site. Of these residues, Glu265(222) was located ~8 Å from the dinuclear zinc(II) active site. The backbone CO of Glu265(222) were hydrogen-bonded to the side chain OG of Ser225(182) at distances of 2.6 Å, but the side chain of Glu265(222) was turned to face the surface of the protein. Therefore, the side chain was not likely to influence the catalytic efficiency of IND-5 by Glu-to-Asp substitution at position 265. One possibility affecting the enzymatic activity of the mutant might have been the residue at position 235 (BBL numbering), which was located almost on top of loop 2 at a distance of ~9 Å from Zn1 and Zn2. In IND-1, IND-5 and IND-7, the residue at position 235 was Lys, whereas, for IND-2 the residue at the same position was Gly. Lys235(192) in the IND-7 structure had a strained main chain conformation, with ϕ and ψ angles of -60° and -29°, respectively. However, the Lys-to-Gly substitution at position 235 in IND-2 may have increased the degree of rotation about the ϕ and ψ angles, compared with IND-5, and caused the movement of loop 2 to access the conserved residue in all IND variants, Tyr233(190), of the hydrophobic pocket. Thus, the mutation at position 235 appeared to trigger changes in the mobility of the loop and in the uptake of the substrate to the active site, leading to a difference in the enzymatic activity.

In conclusion, we determined the crystal structure of IND-7 metallo-β-lactamase of *C. indologenes*. As a consequence, the precise coordination mode around the dinuclear zinc(II) active site was ascertained, and its coordination mode appeared to be quite different from those of the well-characterized metallo-β-lactamases, as determined by X-ray crystallography. It was predicted that the hydrogen-bonding interaction between Arg121(101) and Gly262(219) would influence conformational flexibility of His263(220) and, as the result, the fixation of His263(220) to Zn2 by this interaction did contribute to the binding affinity of Zn2 and to the enzymatic performance. Finally, the residue at position 235 of loop 2, rather than Glu-to-Asp substitution at position 265, might be critical to altering the enzymatic activity in the IND variants.

Funding

Aspects of the present study related to cloning, overexpression, purification, crystal optimization and X-ray diffraction analysis of the enzyme were supported by Grants from the Ministry of Health, Labor, and Welfare of Japan (H18-Shinkou-11 and H21-Shinkou-Ippan-008). A preliminary X-ray crystallographic analysis was supported by a Grant from the Ohyama Health Foundation, Inc. (to Y. Yamaguchi).

Conflict of interest

None declared.

References

1. Fisher, J.F., Meroueh, S.O., and Mobashery, S. (2005) Bacterial resistance to β-lactam antibiotics: Compelling opportunism, compelling opportunity. *Chem. Rev.* **105**, 395–424
2. Frère, J.-M. (1995) Beta-lactamases and bacterial resistance to antibiotics. *Mol. Microbiol.* **16**, 385–395
3. Wilke, M.S., Lovering, A.L., and Strynadka, N.C. (2005) Beta-lactam antibiotic resistance: a current structural perspective. *Curr. Opin. Microbiol.* **8**, 525–533
4. Galleni, M., Lamotte-Brasseur, J., Rossolini, G.M., Spencer, J., Dideberg, O., and Frère, J.-M. The metallo-β-lactamase working group. (2001) Standard numbering scheme for class B β-lactamases. *Antimicrob. Agents Chemother.* **45**, 660–663
5. Garau, G., Di Guilmi, A.M., and Hall, B.G. (2005) Structure-based phylogeny of the metallo-β-lactamases. *Antimicrob. Agents Chemother.* **49**, 2778–2784
6. Rasmussen, B.A. and Bush, K. (1997) Carbapenem-hydrolyzing β-lactamases. *Antimicrob. Agents Chemother.* **41**, 223–232
7. Fabiane, S.M., Sohi, M.K., Wan, T., Payne, D.J., Bateson, J.H., Mitchell, T., and Sutton, B.J. (1998) Crystal structure of the zinc-dependent β-lactamase from *Bacillus cereus* at 1.9 Å resolution: binuclear active site with features of a mononuclear enzyme. *Biochemistry* **37**, 12404–12411
8. Toney, J.H., Hammond, G.G., Fitzgerald, P.M.D., Sharma, N., Balkovec, J.M., Rouen, G.P., Olson, S.H., Hammond, M.L., Greenlee, M.L., and Gao, Y.-D. (2001) Succinic acids as potent inhibitors of plasmid-borne IMP-1 metallo-β-lactamase. *J. Biol. Chem.* **276**, 31913–31918
9. García-Sáez, I., Mercuri, P.S., Papamicael, C., Kahn, R., Frère, J.-M., Galleni, M., Rossolini, G.M., and Dideberg, O. (2003) Three-dimensional structure of FEZ-1, a monomeric subclass B3 metallo-β-lactamase from *Fluoribacter gormanii,* in native form and in complex with D-captopril. *J. Mol. Biol.* **325**, 651–660
10. Murphy, T.A., Catto, L.E., Halford, S.E., Hadfield, A.T., Minor, W., Walsh, T.R., and Spencer, J. (2006) Crystal structure of *Pseudomonas aeruginosa* SPM-1 provides insights into variable zinc affinity of metallo-β-lactamases. *J. Mol. Biol.* **357**, 890–903
11. Felici, A., Amicosante, G., Oratore, A., Strom, R., Ledent, P., Joris, B., Fanuel, L., and Frère, J.-M. (1993) An overview of the kinetic parameters of class B β-lactamases. *Biochem. J.* **291**, 151–155
12. Garau, G., Bebrone, C., Anne, C., Galleni, M., Frère, J.M., and Dideberg, O. (2005) A metallo-β-lactamase enzyme in action: crystal structures of the monozinc carbapenemase CphA and its complex with biapenem. *J. Mol. Biol.* **345**, 785–795
13. Sharma, N.P., Hajdin, C., Chandrasekar, S., Bennett, B., Yang, K.W., and Crowder, M.W. (2006) Mechanistic studies on the mononuclear Zn(II)-containing metallo-β-lactamase ImiS from *Aeromonas sobria*. *Biochemistry* **45**, 10729–10738
14. Crawford, P.A., Yang, K.W., Sharma, N., Bennett, B., and Crowder, M.W. (2005) Spectroscopic studies on cobalt(II)-substituted metallo-β-lactamase ImiS from *Aeromonas veronii* bv. *sobria*. *Biochemistry* **44**, 5168–5176
15. Bebrone, C., Anne, C., De Vriendt, K., Devreese, B., Rossolini, G.M., Van Beeumen, J., Frere, J.M., and Galleni, M. (2005) Dramatic broadening of the substrate profile of the *Aeromonas hydrophila* CphA metallo-β-lactamase by site-directed mutagenesis. *J. Biol. Chem.* **280**, 28195–28202
16. Walsh, T.R., Gamblin, S., Emery, D.C., MacGowan, A.P., and Bennett, P.M. (1996) Enzyme kinetics and biochemical analysis of ImiS, the metallo-β-lactamase from *Aeromonas sobria* 163a. *J. Antimicrob. Chemother.* **37**, 423–431
17. Segatore, B., Massidda, O., Satta, G., Setacci, D., and Amicosante, G. (1993) High specificity of *cphA*-encoded metallo-β-lactamase from *Aeromonas hydrophila* AE036 for carbapenems and its contribution to β-lactam resistance. *Antimicrob. Agents Chemother.* **37**, 1324–1328
18. Walsh, T.R., Toleman, M.A., Poirel, L., and Nordmann, P. (2005) Metallo-β-lactamases: the quiet before the storm? *Clin. Microbiol. Rev.* **18**, 306–325
19. Senda, K., Arakawa, Y., Ichiyama, S., Nakashima, K., Ito, H., Ohsuka, S., Shimokata, K., Kato, N., and Ohta, M. (1996) PCR detection of metallo–βlactamase gene (blaIMP) in gram-negative rods resistant to broad-spectrum β-lactams. *J. Clin. Microbiol.* **34**, 2909–2913
20. Lauretti, L., Riccio, M.L., Mazzariol, A., Cornaglia, G., Amicosante, G., Fontana, R., and Rossolini, G.M. (1999) Cloning and characterization of bla_{VIM}, a new integron-borne metallo-β-lactamase gene from a *Pseudomonas aeruginosa* clinical isolate. *Antimicrob. Agents Chemother.* **43**, 1584–1590
21. Lim, H.M., Pene, J.J., and Shaw, R.W. (1988) Cloning, nucleotide sequence, and expression of the *Bacillus cereus* 5/B/6 β-lactamase II structural gene. *J. Bacteriol.* **170**, 2873–2878
22. Rossolini, G.M., Franceschini, N., Lauretti, L., Caravelli, B., Riccio, M.L., Galleni, M., Frère, J.M., and Amicosante, G. (1999) Cloning of a *Chryseobacterium* (*Flavobacterium*) *meningosepticum* chromosomal gene ($blaA_{(CME)}$) encoding an extended-spectrum class A β-lactamase related to the *Bacteroides cephalosporinases* and the VEB-1 and PER β-lactamases. *Antimicrob. Agents Chemother.* **43**, 2193–2199
23. Wang, Z., Fast, W., and Benkovic, S.J. (1998) Direct observation of an enzyme-bound intermediate in the catalytic cycle of the metallo-β-lactamase from *Bacteroides fragilis*. *J. Am. Chem. Soc.* **120**, 10778–10789
24. Bellais, S., Léotard, S., Poirel, L., Naas, T., and Nordmann, P. (1999) Molecular characterization of a carbapenem-hydrolyzing β-lactamase from *Chryseobacterium* (*Flavobacterium*) *indologenes*. *FEMS Microbiol. Lett.* **171**, 127–132
25. Osano, E., Arakawa, Y., Wacharotayankun, R., Ohta, M., Horii, T., Ito, H., Yoshimura, F., and Kato, N. (1994) Molecular characterization of an enterobacterial metallo β-lactamase found in a clinical isolate of *Serratia marcescens* that shows imipenem resistance. *Antimicrob. Agents Chemother.* **38**, 71–78
26. Toleman, M.A., Simm, A.M., Murphy, T.A., Gales, A.C., Biedenbach, D.J., Jones, R.N., and Walsh, T.R. (2002) Molecular characterization of SPM-1, a novel metallo-β-lactamase isolated in Latin America: report from the SENTRY antimicrobial surveillance programme. *J. Antimicrob. Chemother.* **50**, 673–679
27. Castanheira, M., Toleman, M.A., Jones, R.N., Schmidt, F.J., and Walsh, T.R. (2004) Molecular characterization of a β-lactamase gene, bla_{GIM-1}, encoding a new subclass of metallo-β-lactamase. *Antimicrob. Agents Chemother.* **48**, 4654–4661
28. Carfi, A., Pares, S., Duée, E., Galleni, M., Duez, C., Frère, J.-M., and Dideberg, O. (1995) The 3-D structure

of a zinc metallo-β-lactamase from *Bacillus cereus* reveals a new type of protein fold. *EMIBO J*. **14**, 4914–4921
29. Carfi, A., Duee, E., Galleni, M., Frère, J.-M., and Dideberg, O. (1998) 1.85 Å resolution structure of the zinc (II) β-lactamase from *Bacillus cereus*. *Acta Cryst*. **D54**, 313–323
30. Chantalat, L., Duée, E., Galleni, M., Frère, J.M., and Dideberg, O. (2000) Structural effects of the active site mutation cysteine to serine in *Bacillus cereus* zinc-β-lactamase. *Protein Sci*. **9**, 1402–1406
31. García-Sáez, I., Hopkins, J., Papamicael, C., Franceschini, N., Amicosante, G., Rossolini, G.M., Galleni, M., Frère, J.-M., and Dideberg, O. (2003) The 1.5-Å structure of *Chryseobacterium meningosepticum* zinc β-lactamase in complex with the inhibitor, D-captopril *J. Biol. Chem*. **278**, 23868–23873
32. Concha, N.O., Rasmussen, B.A., Bush, K., and Herzberg, O. (1996) Crystal structure of the wide-spectrum binuclear zinc β-lactamase from *Bacteroides fragilis*. *Structure* **4**, 823–836
33. Carfi, A., Duée, E., Paul-Soto, R., Galleni, M., Frère, J.-M., and Dideberg, O. (1998) X-ray structure of the ZnII β-lactamase from *Bacteroides fragilis* in an orthorhombic crystal form. *Acta Cryst*. **D54**, 45–57
34. Fitzgerald, P.M.D., Wu, J.K., and Toney, J.H. (1998) Unanticipated inhibition of the metallo-β-lactamase from *Bacteroides fragilis* by 4-morpholineethanesulfonic acid (MES): A crystallographic study at 1.85-Å resolution. *Biochemistry* **37**, 6791–6800
35. Concha, N.O., Janson, C.A., Rowling, P., Pearson, S., Cheever, C.A., Clarke, B.P., Lewis, C., Galleni, M., Frère, J.-M., Payne, D.J., Bateson, J.H., and Abdel-Meguid, S.S. (2000) Crystal structure of the IMP-1 metallo β-lactamase from *Pseudomonas aeruginosa* and its complex with a mercaptocarboxylate inhibitor: binding determinants of a potent, broad-spectrum inhibitor. *Biochemistry* **39**, 4288–4298
36. Kurosaki, H., Yamaguchi, Y., Yasuzawa, H., Jin, W., Yamagata, Y., and Arakawa, Y. (2006) Probing, inhibition, and crystallographic characterization of metallo-β-lactamase (IMP-1) with fluorescent agents containing dansyl and thiol groups. *Chem. Med. Chem*. **1**, 969–972
37. Garcia-Saez, I., Docquier, J.D., Rossolini, G.M., and Dideberg, O. (2008) The three-dimensional structure of VIM-2, a Zn-β-lactamase from *Pseudomonas aeruginosa* in its reduced and oxidised form. *J. Mol. Biol*. **375**, 604–611
38. Yamaguchi, Y., Jin, W., Matsunaga, K., Ikemizu, S., Yamagata, Y., Wachino, J., Shibata, N., Arakawa, Y., and Kurosaki, H. (2007) Crystallographic investigation of the inhibition mode of a VIM-2 metallo-β-lactamase from *Pseudomonas aeruginosa* by a mercaptocarboxylate inhibitor. *J. Med. Chem*. **50**, 6647–6653
39. Bellais, S., Poirel, L., Leotard, S., Naas, T., and Nordmann, P. (2000) Genetic diversity of carbapenem-hydrolyzing metallo-β-lactamases from *Chryseobacterium* (*Flavobacterium*) *indologenes*. *Antimicrob. Agents Chemother*. **44**, 3028–3034
40. Perilli, M., Caporale, B., Celenza, G., Pellegrini, C., Docquier, J.D., Mezzatesta, M., Rossolini, G.M., Stefani, S., and Amicosante, G. (2007) Identification and characterization of a new metallo-β-lactamase, IND-5, from a clinical Isolate of *Chryseobacterium indologenes*. *Antimicrob. Agents Chemother*. **51**, 2988–2990
41. Zeba, B., De Luca, F., Dubus, A., Delmarcelle, M., Simporé, J., Nacoulma, O.G., Rossolini, G.M., Frère, J.-M., and Docquier, J.-D. (2009) IND-6, a highly divergent IND-type metallo-β-lactamase from *Chryseobacterium indologenes* strain 597 isolated in Burkina Faso. *Antimicrob. Agents Chemother*. **53**, 4320–4326
42. Hsueh, P.R., Teng, L.J., Ho, S.W., Hsieh, W.C., and Luh, K.T. (1996) Clinical and microbiological characteristics of *Flavobacterium indologenes* infections associated with indwelling devices. *J. Clin. Microbiol*. **34**, 1908–1913
43. Otwinowski, Z. and Minor, W. (1997) Processing of X-ray diffraction data collected in oscillation mode *Methods Enzymol. 276,* 307–326
44. Navaza, J. (1994) *AMoRe*: an automated package for molecular replacement. *Acta Cryst*. **A50**, 157–163
45. Vagin, A. and Teplyakov, A. (1997) *MOLREP*: an automated program for molecular replacement. *J. Appl. Cryst*. **30**, 1022–1025
46. Collaborative Computational Project Number 4. (1994) The CCP4 suite: Programs for protein crystallography. *Acta Cryst*. **D50**, 760–763
47. Jones, T.A., Zou, J.-Y., Cowan, S.W., and Kjeldgaard, M. (1991) Improved methods for building protein models in electron density maps and the location of errors in these models. *Acta Cryst*. **A47**, 110–119
48. Emsley, P. and Cowtan, K. (2004) *Coot*: model-building tools for molecular graphics. *Acta Cryst*. **D60**, 2126–2132
49. Brünger, A.T., Adams, P.D., Clore, G.M., DeLano, W.L., Gros, P., Grosse-Kunstleve, R.W., Jiang, J.-S., Kuszewski, J., Nilges, M., Pannu, N.S., Read, R.J., Rice, L.M., Simonson, T., and Warren, G.L. (1998) *Crystallography & NMR system*: a new software suite for macromolecular structure determination. *Acta Cryst*. **D54**, 905–921
50. Murshudov, G.N., Vagin, A.A., and Dodson, E.J. (1997) Refinement of macromolecular structures by the maximum-likelihood method. *Acta Cryst*. **D53**, 240–255
51. Moali, C., Anne, C., Lamotte-Brasseur, J., Groslambert, S., Devreese, B., Van Beeumen, J., Galleni, M., and Frère, J.-M. (2003) Analysis of the importance of the metallo-β-lactamase active site loop in substrate binding and catalysis. *Chem. Biol*. **10**, 319–329
52. Huntley, J.J.A., Scrofani, S.D.B., Osborne, M.J., Wright, P.E., and Dyson, H.J. (2000) Dynamics of the metallo-β-lactamase from *Bacteroides fragilis* in the presence and absence of a tight-binding inhibitor. *Biochemistry* **39**, 13356–13364
53. Huntley, J.J., Fast, W., Benkovic, S.J., Wright, P.E., and Dyson, H.J. (2003) Role of a solvent-exposed tryptophan in the recognition and binding of antibiotic substrates for a metallo-β-lactamase. *Protein Sci*. **12**, 1368–1375
54. Scrofani, S.D.B., Chung, J., Huntley, J.J.A., Benkovic, S.J., Wright, P.E., and Dyson, H.J. (1999) NMR characterization of the metallo-β-lactamase from *Bacteroides fragilis* and its interaction with a tight-binding inhibitor: role of an active-site loop. *Biochemistry* **38**, 14507–14514
55. Salsbury, F.R. Jr, Crowley, M.F., and Brooks, C.L. III. (2001) Modeling of the metallo-β-lactamase from *B. fragilis*: structural and dynamic effects of inhibitor binding. *Proteins: Struct., Funct., Genet*. **44**, 448–459
56. Addison, A.W., Rao, T.N., Reedijk, J., van Rijn, J., and Verschoor, G.C. (1984) Synthesis, structure, and spectroscopic properties of copper(II) compounds containing nitrogen–sulphur donor ligands; the crystal and molecular structure of aqua[1,7-bis(N-methylbenzimidazol-2-yl)-2,6-dithiaheptane]copper(II) perchlorate. *J. Chem. Soc., Dalton Trans*. 1349–1356
57. Ullah, J.H., Walsh, T.R., Taylor, I.A., Emery, D.C., Verma, C.S., Gamblin, S.J., and dand Spencer, J. (1998) The crystal structure of the L1 metallo-

β-lactamase from *Stenotrophomonas maltophilia* at 1.7 Å resolution. *J. Mol. Biol.* **284**, 125–136
58. Wang, Z., Fast, W., Valentine, A.M., and Benkovic, S.J. (1999) Metallo-β-lactamase: Structure and mechanism. *Curr. Opin. Chem. Biol.* **3**, 614–622
59. Tamames, B., Sousa, S.F., Tamames, J., Fernandes, P.A., and Ramos, M.J. (2007) Analysis of zinc-ligand bond lengths in metalloproteins: trends and patterns. *Proteins* **69**, 466–475
60. Rossolini, G.M., Franceschini, N., Riccio, M.L., Mercuri, P.S., Perilli, M., Gaalleni, M., Frère, J.-M., and Amicosante, G. (1998) Characterization and sequence of the *Chryseobacterium* (*Flavobacterium*) *meningosepticum* carbapenemase: a new molecular class B β-lactamase showing a broad substrate profile. *Biochem. J.* **332**, 145–152
61. Orellano, E.G., Girardini, J.E., Cricco, J.A., Ceccarelli, E.A., and Vila, A.J. (1998) Spectroscopic characterization of a binuclear metal site in *Bacillus cereus* β-lactamase II. *Biochemistry* **37**, 10173–10180
62. Davies, R.B. and Abraham, E.P. (1974) Metal cofactor requirements of β-lactamase II. *Biochem. J.* **143**, 129–135
63. Baldwin, G.S., Galdes, A., Hill, H.A., Smith, B.E., Waley, S.G., and Abraham, E.P. (1978) Histidine residues of zinc ligands in β-lactamase II. *Biochem. J.* **175**, 441–447
64. Crowder, M.W., Wang, Z., Franklin, S.L., Zovinka, E.P., and Benkovic, S.J. (1996) Characterization of the metal-binding sites of the β-lactamase from *Bacteroides fragilis*. *Biochemistry* **35**, 12126–12132
65. Laraki, N., Franceschini, N., Rossolini, G.M., Santucci, P., Meunier, C., de Pauw, E., Amicosante, G., Frère, J.M., and Galleni, M. (1999) Biochemical characterization of the *Pseudomonas aeruginosa* 101/1477 metallo-β-lactamase IMP-1 produced by *Escherichia coli*. *Antimicrob. Agents Chemother.* **43**, 902–906
66. Corpet, F. (1988) Multiple sequence alignment with hierarchical clustering. *Nucleic Acids Res.* **16**, 10881–10890